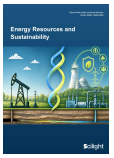
Energy Resources and Sustainability
https://www.sciltp.com/journals/eras



Article

Carbonization of Lignite Coal and Leonardite through Pyrolysis for Sustainable Post-Combustion Applications

Hussameldin Ibrahim * and Jephthah T. Ofoe

Clean Energy Technologies Research Institute (CETRI), Process Systems Engineering, Faculty of Engineering & Applied Science, University of Regina, 3737 Wascana Parkway, Regina, SK S4S 0A2, Canada
* Correspondence: hussameldin.ibrahim@uregina.ca

How To Cite: Ibrahim, H.; Ofoe, J.T. Carbonization of Lignite Coal and Leonardite through Pyrolysis for Sustainable Post-Combustion Applications. *Energy Resources and Sustainability* **2026**, *1*(1), 3.

Received: 9 August 2026
Revised: 2 September 2026
Accepted: 7 September 2026
Published: 4 November 2026

Abstract: This study investigates the carbonization behavior of Saskatchewan-sourced lignite coal and leonardite through controlled pyrolysis at 450 °C, 650 °C, and 850 °C, with residence times of 30, 75, and 120 min. The influence of temperature and time on product distribution, reaction pathways, and char properties was systematically evaluated to inform sustainable valorization strategies. Char yields decreased progressively with increasing temperature and time, while liquid yields peaked at 650 °C before declining at higher temperatures. Gas production was maximized at 850 °C, with temperature exerting a more pronounced effect on yield distribution than time, attributed to temperature's role in initiating the various pyrolytic reactions. In contrast, time only impacted the extent of these reactions. Although char yields from both feedstocks were comparable across all conditions, Leonardite consistently produced more gas, whereas lignite yielded more liquid products. Kinetic analysis via the Coats-Redfern method effectively modeled pyrolysis under first-order assumptions up to 700 °C, revealing lower apparent activation energies for leonardite (5–26 kJ/mol) compared to lignite (12–32 kJ/mol) across two devolatilization phases (Stages 1 & 2) due to its weathered, oxygen-dense structure. While higher-order models (second and third orders) and elevated thermal regimes (700–800 °C) modeled complex reactions, lower correlation coefficients (R^2 < 0.98) and drastically elevated activation energies (surpassing 250 kJ/mol) of these models highlighted the limitations of classical model-fitting in isolating true chemical kinetics under complex mass-transfer constraints. The findings provide critical insights into the thermochemical conversion of low-rank coals and oxidized humic substances, offering a foundation for their tailored use in carbon-based materials, adsorbents, and energy applications.

Keywords: pyrolysis; temperature; time; product pathways; product distributions

1. Introduction

As global carbon management strategies pivot toward sustainable materials and cleaner energy systems, thermochemical conversion processes like pyrolysis have emerged as vital pathways for upgrading low-value carbonaceous feedstocks [1]. Pyrolysis involves the thermal decomposition of organic matrices in oxygen-free environments, allowing for the co-production of solid char, condensable liquids, and non-condensable syngas [2]. In the context of localized resource optimization, low-rank coals and related organic deposits represent massive, underutilized precursors for carbonaceous products [3–5]. Extensive deposits of lignite coal and its naturally oxidized derivative, leonardite, provide a unique opportunity to evaluate how varying degrees of geological weathering alter pyrolytic reaction pathways and product yields [6].



Copyright: © 2026 by the authors. This is an open access article under the terms and conditions of the Creative Commons Attribution (CC BY) license (https://creativecommons.org/licenses/by/4.0/).
Publisher's Note: Scilight stays neutral with regard to jurisdictional claims in published maps and institutional affiliations.

Lignite is characterized by a complex, low-rank, cross-linked organic framework. When subjected to severe environmental weathering and intense oxidation over geological timescales, it transforms into leonardite, a highly oxidized, humic-acid-rich substance [7,8]. While both feedstocks share a common sedimentary ancestry, this extensive natural oxidation profoundly alters their chemical bonds, thermal stability, and overall composition. Specifically, geological weathering cleaves heavy aromatic precursors and enriches the matrix with oxygen-containing functional groups (such as carboxylic, phenolic, and ethereal structures), fundamentally shifting the material from a traditional hydrocarbon skeleton to an oxygen-dense humic network. Consequently, when subjected to artificial thermal stress during pyrolysis, these two materials are expected to follow fundamentally different decomposition mechanisms [7]. Unweathered lignite typically favors the cleavage of weak aliphatic bridges leading to tar formation, whereas the pre-oxidized, oxygen-rich matrix of leonardite is hypothesized to undergo accelerated radical scission, lower activation energy barriers, and suppress condensable liquid yields in favor of permanent gas evolution [9].

Evaluating these two co-located feedstocks side-by-side provides a unique scientific framework to isolate the role of natural weathering on thermochemical behavior under identical reactor conditions. A significant gap remains in the literature regarding the direct, comparative kinetic and yield behavior of co-located lignite and leonardite deposits. While standard coal pyrolysis has been widely documented, the thermochemical conversion of highly oxidized humic substances like leonardite is frequently overlooked or generalized to match conventional low-rank coals [10–13]. For instance, the combined, interactive effects of peak pyrolysis temperature and holding residence time on the product distribution between solid, liquid, and gas phases for these two distinct feedstocks have not been systematically unraveled. Furthermore, quantifying the difference in the energy barriers (activation energies) required to initiate thermal decomposition for a weathered versus an unweathered matrix is critical for process scaling and reactor design.

To address these gaps, this study investigates the devolatilization behavior of lignite and leonardite via controlled pyrolysis. This work examines how natural oxidation dictates volatile phase splitting and char reactivity by directly comparing their product yield distributions, activation energies, and char structural transformations, to provide a predictive foundation for the tailored thermochemical valorization of lignite and leonardite into specialized carbon-based materials and energy applications.

2. Methods

2.1. Pyrolysis Experimental Procedure

Pyrolysis experiments were conducted in a sliding tube furnace (Figure 1). For each experimental run, 5 g of dried sample feedstock (leonardite and lignite) was weighed using a mass balance (error = 0.001 g) into a boat-like crucible and positioned within the furnace's heating zone. Prior to each pyrolysis experiment, atmospheric air was evacuated from the quartz tube using a vacuum pump, followed by introducing nitrogen gas at 300 mL/min to establish an inert, oxygen-free atmosphere. The experiments were conducted at target temperatures of 450, 650, and 850 °C, ramping up at 10 °C/min from room temperature. Isothermal residence times of 30, 75, and 120 min were initiated once the reactor zone reached the target set-point temperature, ensuring a consistent and reproducible thermal history across all experimental runs. All experimental runs were performed at least in duplicate, maintaining a relative deviation within ± 5%. The mass yields of the solid, liquid, and gaseous phases produced during pyrolysis were quantified on a mass percentage basis relative to the initial dry feedstock using the following equations:

$$\mathrm{Y_{char}} = \frac{\mathrm{m_{char}}}{\mathrm{m_{coal}}} \times 100 \quad (1)$$

$$\mathrm{Y_{LP}} = \frac{\mathrm{m_{LP}}}{\mathrm{m_{coal}}} \times 100 \quad (2)$$

$$\mathrm{Y_{gas}} = 100 - \mathrm{Y_{char}} - \mathrm{Y_{LP}} \quad (3)$$

where:

Y_{char} = the yield of char (wt%);
Y_{LP} = liquid products yield, including water (wt%);
Y_{gas} = gas yield (wt%);
m_{char} = char mass (g);
m_{coal} = coal mass (g);
m_{LP} = mass of liquid products (g).

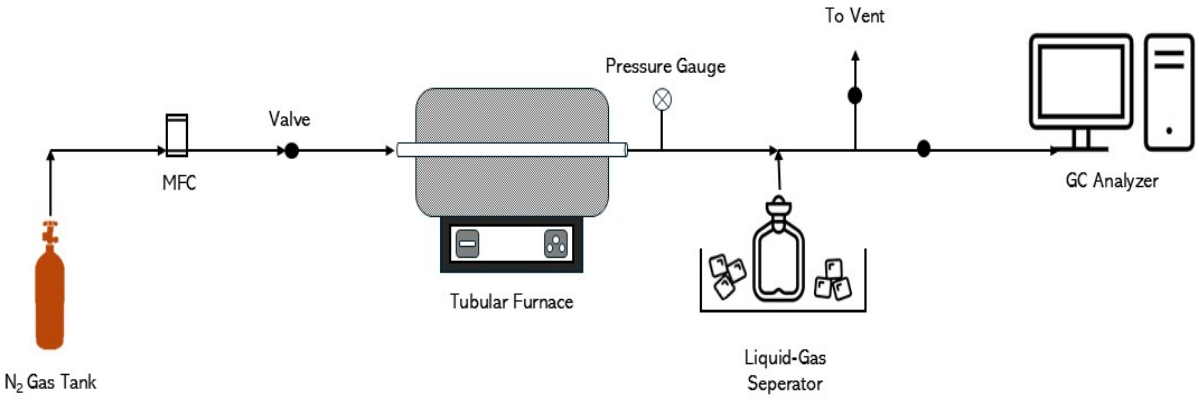


Figure 1. Schematic diagram of the setup for pyrolysis experiments.

2.2. Characterization of Pyrolysis Products

The physical and chemical evolutions of the solid char products obtained across the varying pyrolysis temperatures and residence times were systematically evaluated using ultimate and textural analyses.

2.2.1. Ultimate Analysis (Elemental Composition)

The elemental composition (C, H, N, and S content) of the resulting chars was determined using a Vario EL III CHNS Elemental Analyzer (Elementar Americas, Inc., Ronkonkoma, NY, USA) to monitor carbon enrichment and heteroatom elimination dynamics during thermal carbonization. The fixed oxygen content of the chars was calculated by difference based on mass balance:

$$\text{Oxygen} = 100 - (\text{C} + \text{H} + \text{N} + \text{S} + \text{Ash}) \quad (4)$$

2.2.2. Textural and Structural Pore Evolution

The evolution of the char pore structure, including specific surface area, total pore volume, and average pore diameter, was characterized via N_2 physisorption at 77 K using a MicroActive 3FLEX 3500 instrument (Micromeritics Instrument Inc., Norcross, GA, USA). Before the adsorption-desorption measurements, approximately 300 mg of the char sample was degassed under a vacuum at 145 °C for 24 h to remove any residual moisture or trapped volatile matter from the pore networks. The specific surface areas of the chars were calculated by applying the Brunauer-Emmett-Teller (BET) equation, while the evolution of the pore volumes and pore size distributions was modeled from the desorption isotherms using the Barrett-Joyner-Halenda (BJH) method.

2.3. Macro-Kinetic Modeling of Pyrolysis

To evaluate the energy barriers governing the thermal decomposition of lignite and leonardite, the model-fitting technique was used. The integral method with the Coats-Redfern approximation was employed. Details of the derivations are provided elsewhere [14,15]. Thermogravimetric (TG) mass loss data were acquired across the main devolatilization zone using an array of constant heating rates: 5, 10, 20, and 30 °C/min.

In accordance with established protocols for low-rank coal pyrolysis kinetics, the initial low-temperature dehydration stage was omitted from the kinetic calculations [16]. This isolates the core pyrolytic devolatilization phenomena, specifically the cracking of weak aliphatic bridges, functional group elimination, and structural carbonization, ensuring that moisture evaporation dynamics do not interfere with the determination of true chemical kinetic parameters [17].

3. Results and Discussion

3.1. Pyrolysis Product Distribution and Yield Profiles

The evolution of solid (char), liquid (condensable volatiles), and gaseous product yields as a function of temperature and isothermal holding times for lignite and leonardite are presented in Figures 2 and 3. The experimental data revealed that while temperature governs the thermodynamic viability of specific bond-cleavage regimes, the residence time determines the kinetic extent of these reactions.

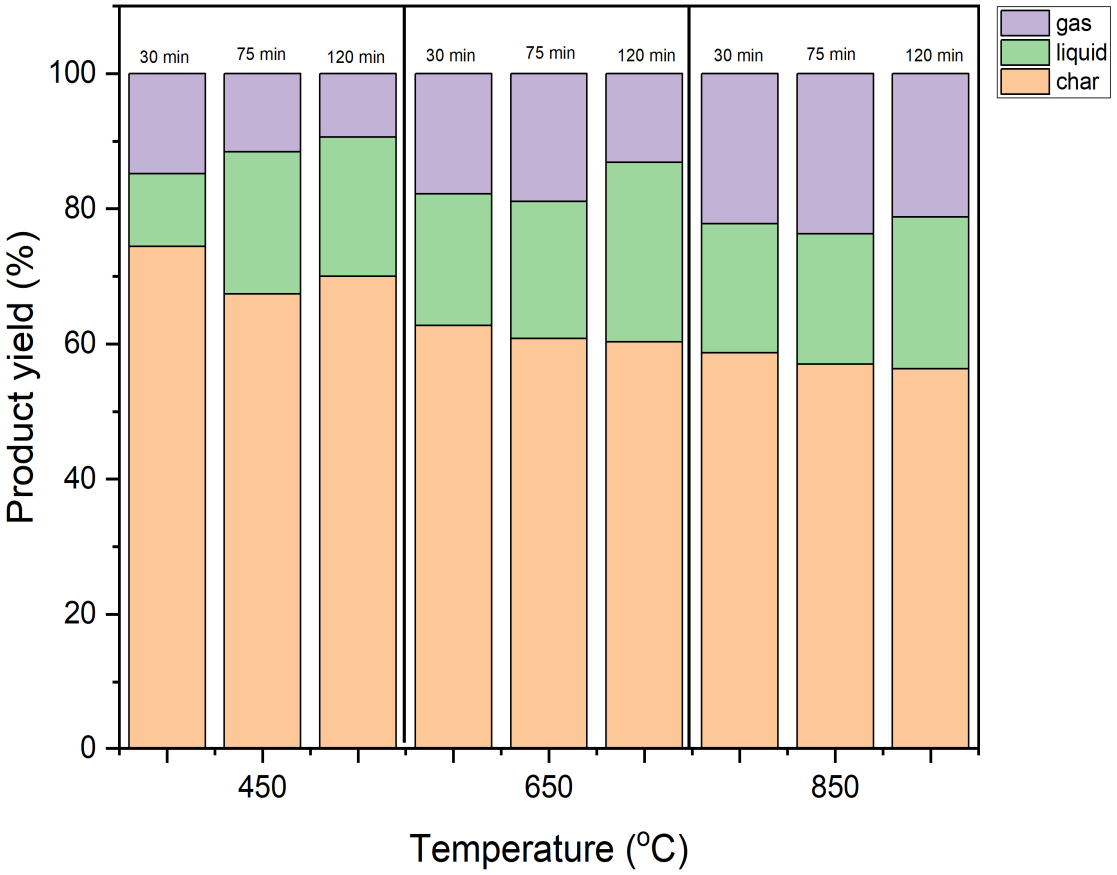


Figure 2. Phase distribution of the pyrolysis products of lignite at different temperatures and times on dry basis, with each experiment performed two times and deviations within ±5 wt%.

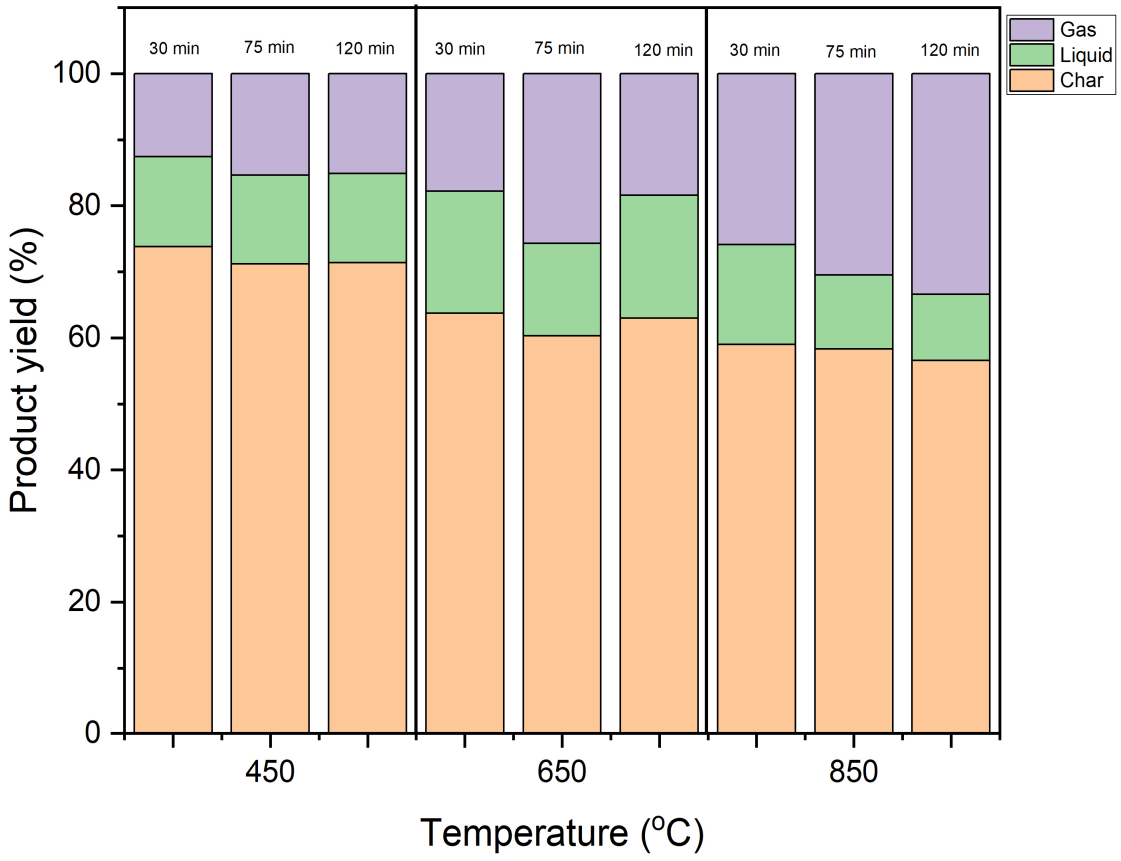


Figure 3. Phase distribution of the pyrolysis products of leonardite at different temperatures and times on dry basis, with each experiment performed two times and deviations within ±5 wt%.

3.1.1. Solid Char Yield Dynamics

For both feedstocks, the experimentally measured solid char yield decreased monotonically as the pyrolysis temperature increased. At 450 °C, char yields remained relatively high, recording 74.4 wt% for lignite at a 30-min residence time. As the temperature was raised to 850 °C, char yields declined significantly, dropping to 56.3 wt% for lignite at 120 min. These trends align with established principles of coal pyrolysis. The relatively high char yield at 450 °C indicates that thermal energy at this lower threshold was primarily sufficient only to initiate the cleavage of weak aliphatic linkages (such as C–O, C–C, and C–H bridges) [2,18]. In agreement with literature models, this homolytic cleavage generates reactive free radicals that undergo structural rearrangement into localized aromatic complexes rather than diffusing out of the matrix [18,19]. The subsequent decline in char yield at 850 °C is attributed to the thermal cracking of stable aromatic clusters, polycondensation, and the release of tightly bound residual volatiles.

The influence of isothermal residence time varied depending on the thermal window. For instance, extending the holding time at 450 °C from 30 to 75 min noticeably reduced the lignite char yield from 74.4 wt% to 67.4 wt%. However, at elevated temperatures (650 °C and 850 °C), the rate of yield decrease slowed significantly. Mechanistically, this behavior implies that primary devolatilization reactions approached equilibrium rapidly at higher temperatures, thereby minimizing time dependency [9].

An interesting anomaly was observed at 450 °C and 120 min, where a slight upturn in yield occurred. This behavior is interpreted as prolonged thermal exposure encouraging minor solid-phase cross-linking and the rearrangement of heavily depolymerized fragments back into the char skeleton rather than escaping as tar, supported by literature on structural transformations.

3.1.2. Liquid and Gaseous Volatile Evolution

The liquid yield (consisting of tar and reaction water) exhibited a distinct parabolic profile, peaking at 650 °C for both samples before declining at higher temperatures. Experimentally, within this primary devolatilization window up to 650 °C, extending the residence time significantly boosted liquid collection (e.g., increasing from 19.5 wt% to 26.6 wt% for lignite). When temperature was increased to 850 °C, liquid yield dropped sharply while the gas yield reached its maximum.

While these quantitative yield trends directly demonstrate a mass shift from condensable liquids to permanent gases at elevated temperatures, the specific underlying mechanism can be interpreted through established pyrolytic principles. This inverse relationship between liquid and gas yields at 850 °C strongly implies that secondary gas-phase cracking occurs within the bed, consistent with the general coal pyrolysis literature. Under this interpretive framework, tar vapors undergo thermal cracking into light non-condensable permanent gases, releasing carbon monoxide from ether structures, methane from peripheral methyl groups, and hydrogen via aromatic ring condensation. Furthermore, the temporal decrease in gas yield observed for lignite between 75 and 120 min at 850 °C aligns with literature models suggesting the consumption of molecular hydrogen during the stabilization of escaping radical fragments, which shifts product distribution back toward liquid variants [2,9].

3.1.3. Lignite vs. Leonardite Operational Deviations

While solid char yields remained remarkably identical between the two precursors across all configurations, their volatile phase splits deviate fundamentally. Leonardite consistently yielded significantly less condensable liquid but substantially higher gas volumes than lignite. Because leonardite is formed via the intensive natural oxidation of lignite, weathering breaks down heavy aromatic precursors into lighter, oxygen-rich peripheral components, which influenced the volatile evolution during pyrolysis.

This was confirmed at 650 °C, where leonardite gas yields were anomalously high and competitive with their liquid phase yields. Furthermore, at 850 °C, the gas yield of leonardite continued to rise with time (from 25.9 wt% at 30 min to 33.4 wt% at 120 min), avoiding the parabolic profile observed in lignite. This supports the premise that leonardite's volatile structure consists inherently of lighter species that readily undergo secondary gaseous cracking rather than reacting with the solid char substrate.

3.2. Macro-Kinetic Parameters and Reaction Order Modeling

Non-isothermal devolatilization data were fitted using the Coats-Redfern method across first-, second-, and third-order reaction assumptions to isolate the energetics of thermal carbonization. The selection of the most appropriate kinetic model was determined by evaluating the statistical correlation coefficients (R^2) across the experimental heating rates, with models yielding the highest linearity ($R^2 > 0.98$) across the primary

devolatilization windows selected as the most statistically representative [20]. Based on the differential thermogravimetric (DTG) reactivity peaks (Figures 4 and 5), the decomposition pathways were categorized into a three-stage sequence: Stage I (260–560 °C) capturing primary devolatilization, Stage II (560–700 °C) mapping the transition matrix, and Stage III (700–800 °C) corresponding to high-temperature secondary polycondensation.

While absolute apparent activation energy (E_a) values increased systematically with higher assumed reaction orders (Tables 1 and 2) due to the mathematical formulation of the integral method, the first- and second-order models provided the most consistent, physically meaningful fits for the primary devolatilization stages (Stages I and II), reflecting the random scission of weak aliphatic and oxygen-functional bridges widely reported in the literature, and comparing favorably with the activation energies reported by Casal et al. [21]. That said, coal pyrolysis has been widely reported to follow first-order kinetics for model-fitting techniques. As such, the first-order model was primarily used for the comparative evaluation between the two feedstocks.

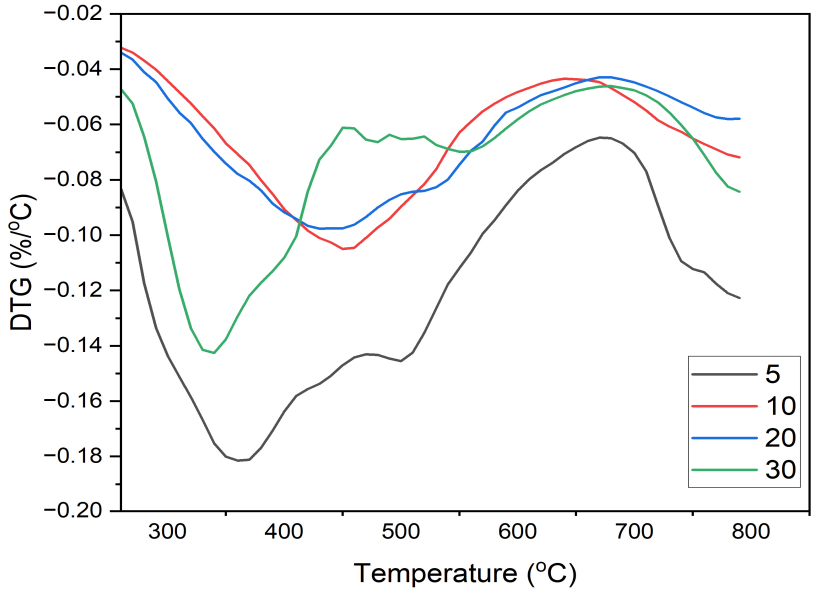


Figure 4. Differential thermogravimetric profiles of lignite at different heating rates.

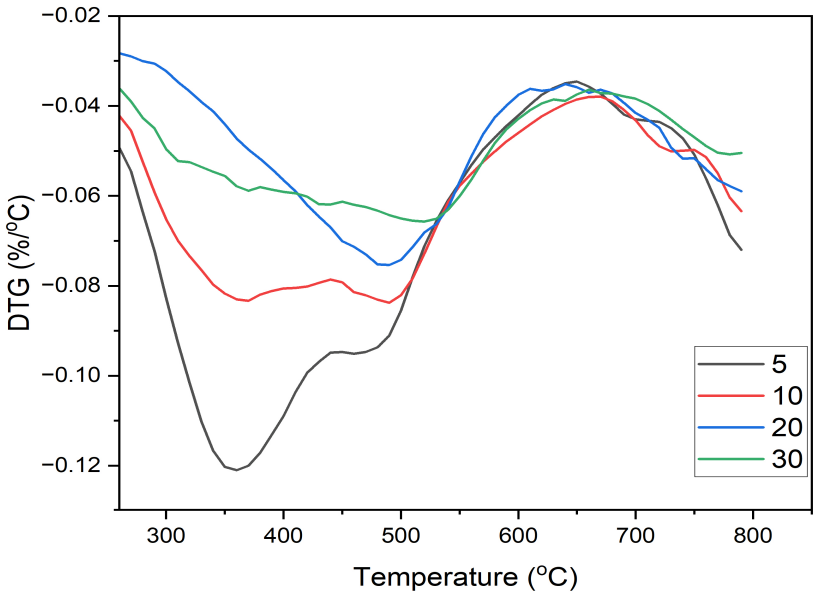


Figure 5. Differential thermogravimetric profiles of leonardite at different heating rates.

A direct analysis of the first-order kinetic parameters reveals clear trends regarding the influence of heating rate and structural differences between the two materials. For both lignite and leonardite, apparent activation energies within equivalent stages tended to increase with rising heating rates (5 to 30 °C/min), a phenomenon typically attributed to heat-transfer limitations and thermal lag within the reacting particle bed at higher thermal ramps [22]. In comparing the two precursors under the first-order assumption, leonardite consistently exhibited

lower apparent activation energy thresholds than lignite across corresponding stages. In Stage I, first-order E_a values for lignite ranged from 12–28 kJ/mol, whereas leonardite values were reduced to 5–12 kJ/mol (Tables 1 and 2). This demonstrates that the abundant oxygen functional groups and weathered aliphatic linkages present in leonardite undergo thermal radical cleavage with a much lower energy barrier than the unweathered lignite coal matrix [23]. In Stage II, activation energies increase for both materials (10–26 kJ/mol for second-order leonardite versus 20–32 kJ/mol for lignite), reflecting the higher energy demand of cracking newly stabilized structural intermediates.

Extending the evaluation to higher-order models provided additional insight into the complex, multi-mechanism nature of coal and humic pyrolysis. The second-order models generally mirrored the stage-wise progression observed in first-order fittings but yielded moderately higher baseline activation energies. In contrast, the third-order assumptions resulted in drastically elevated activation energies and pre-exponential factors, particularly in the higher temperature brackets, where apparent activation energies surged up to 296.69 kJ/mol for lignite and 259.21 kJ/mol for leonardite (Tables 1 and 2).

In the secondary pyrolysis window (700–800 °C), all models yielded steep energetic spikes associated with intensive solid-state polycondensation and ring aromatization. However, the R^2 values dropped significantly, representing a less-than-ideal fit of the Coats-Redfern approximation to the high-temperature pyrolysis dynamics. This may be due to complex mass-transfer limitations, intra-particle gas-phase diffusion, and multi-component condensation kinetics rather than simple single-step bond scission [24]. Consequently, the extreme kinetic parameters, especially third-order fittings at elevated temperatures, indicate that classical model-fitting techniques become less effective in isolating true chemical reaction kinetics in this upper thermal window, reinforcing why first-order models over primary devolatilization ranges are standard for reliable comparative reactivity assessments.

Table 1. The Coats-Redfern kinetic parameters for lignite devolatilization across varied heating rates.

Heating Rate, °C/min	Reaction Order	Temperature Range, °C	Regressed Equation	R^2 Value	E, kJ/mol	A, /min
5	**1st order**	**260–560**	**Y = −1964.2X − 10.796**	**0.9866**	**16.33**	**0.2011**
		550–700	**Y = −2875.5X − 9.1144**	**0.9915**	**26.02**	**2.3659**
		700–790	**Y = −5470.9X − 7.5519**	**0.898**	**31.49**	**14.3642**
	2nd order	260–560	Y = −717.59X − 12.367	0.9992	23.91	1.5825
		560–700	Y = −3130.1X − 8.7911	0.997	5.97	0.0153
	3rd order	260–560	Y = −3947.8X − 6.4611	0.9926	32.82	30.8500
		550–700	Y = −6278.1X − 3.5335	0.9957	52.2	916.682
10	**1st order**	**300–560**	**Y = −1546.3X − 11.409**	**0.9814**	**12.86**	**0.1716**
		560–690	**Y = −2937.8X − 9.0903**	**0.9915**	**24.42**	**3.3125**
		690–790	**Y = −4778.4X − 8.2459**	**0.9077**	**35.73**	**0.1900**
	2nd order	300–560	Y = −2529.1X − 9.647	0.9667	21.03	1.6343
		560–690	Y = −691.19X − 12.435	0.9896	5.75	0.0275
		690–790	Y = −16665X + 4.9739	0.8911	138.55	2.41×10^7
	3rd order	300–560	Y = −3699.3X − 6.8809	0.9529	30.75	38.0000
		550–700	Y = −6045X − 3.9144	0.9836	50.26	1206.1296
		700–790	Y = −35685X + 26.253	0.9003	296.69	9.0×10^{16}
20	**1st order**	**260–560**	**Y = −1489X − 11.471**	**0.9864**	**12.38**	**0.3110**
		560–710	**Y = −3881.7X − 7.9173**	**0.9952**	**32.27**	**28.289**
		710–790	**Y = −4777.9X − 8.2206**	**0.9331**	**39.72**	**25.7100**
	2nd order	280–560	Y = −2401.8X − 9.7966	0.9682	19.97	2.6730
		560–710	Y = −1000.2X − 12.032	0.9904	8.32	0.1190
		710–790	Y = −17848X + 6.1855	0.9249	148.39	1.73×10^8
	3rd order	280–560	Y = −3485.3X − 7.1404	0.9511	28.98	55.2370
		560–710	Y = −7701.5X − 1.8764	0.9882	64.03	23,588.219
		710–790	Y = −35233X + 25.932	0.9246	292.93	1.29×10^{17}
30	**1st order**	**260–420**	**Y = −3314.3X − 8.6817**	**0.9877**	**27.56**	**16.8700**
		420–700	**Y = −2424.3X − 9.8192**	**0.9942**	**20.16**	**3.9560**
		700–790	**Y = −3755X − 9.4004**	**0.9071**	**45.22**	**9.3150**
	2nd order	260–420	Y = −3988X − 7.4075	0.9928	33.16	72.5950
		420–700	Y = −845.87X − 12.348	0.9789	7.03	0.1100
		700–790	Y = −12374X + 0.3477	0.9113	102.88	5.25×10^5
	3rd order	260–420	Y = −4733X − 5.3137	0.9939	39.35	699.1130
		420–700	Y = −4432X − 5.9731	0.9699	36.85	5.22×10^7
		700–790	Y = −23924X + 13.982	0.9123	198.9	8.5×10^{11}

Table 2. The Coats-Redfern kinetic parameters for leonardite devolatilization across varied heating rates.

Heating Rate, °C/min	Reaction Order	Temperature Range, °C	Regressed Equation	R^2 Value	E, kJ/mol	A, /min
5	**1st order**	**260–590**	**Y = −166.35X − 12.831**	**0.9887**	**5.38**	**0.0022**
		590–670	**Y = −1230X − 11.542**	**0.969**	**10.23**	**0.0597**
		670–790	**Y = −2977X − 9.9128**	**0.898**	**24.75**	**0.7374**
	2nd order	260–700	Y = −2448X − 9.2731	0.9908	21.27	1.2012
		700–780	Y = −13,100X + 1.6552	0.9207	26.02	2.3659
	3rd order	260–700	Y = −4183.8X − 5.4522	0.9726	34.78	89.6769
		700–790	Y = −32,641X + 23.753	0.8704	271.38	3.37×10^{15}
10	**1st order**	**260–560**	**Y = −580.05X − 12.44**	**0.9866**	**6.82**	**0.0230**
		560–700	**Y = −935.89X − 12.029**	**0.9915**	**18.78**	**0.0559**
		700–790	**Y = −4226.6X − 8.7284**	**0.9143**	**35.14**	**6.8438**
	2nd order	260–560	Y = −1814.3X − 10.32	0.962	21.28	0.5981
		560–700	Y = −3141.9X − 8.624	0.9904	26.12	5.6472
		700–790	Y = −16,287X + 4.7534	0.9079	135.41	1.89×10^{7}
	3rd order	260–560	Y = −2880.8X − 7.5838	0.9447	23.95	14.6525
		560–700	Y = −6548.8X − 2.9677	0.9896	54.45	3367.49
		700–790	Y = −32,318X + 23.259	0.9085	268.69	4.08×10^{15}
20	**1st order**	**260–570**	**Y = −791.25X − 12.4**	**0.9401**	**9.58**	**0.0652**
		560–700	**Y = −1206.2X − 11.976**	**0.9824**	**24.03**	**0.1518**
		700–790	**Y = −5218.6X − 7.9123**	**0.9428**	**37.39**	**38.2222**
	2nd order	260–700	Y = −2296.8X − 10.027	0.9476	16.11	0.9682
		700–790	Y = −15,692X + 3.7625	0.9196	130.46	1.35×10^{7}
	3rd order	260–700	Y = −3584.7X − 7.0568	0.9239	29.8	61.7666
		700–790	Y = −23,924X + 13.982	0.9123	251.88	4.97×10^{14}
30	**1st order**	**260–570**	**Y = −687.41X − 12.445**	**0.9578**	**11.72**	**1.3012**
		570–700	**Y = −748.83X − 12.318**	**0.9913**	**26.23**	**2.3121**
		700–790	**Y = −4193.9X − 8.8327**	**0.9402**	**41.87**	**18.3551**
	2nd order	260–570	Y = −1402X − 10.997	0.9263	11.66	1.2623
		570–700	Y = −3414.4X − 8.459	0.9893	28.39	3.4745
		700–790	Y = −14,147X + 2.4597	0.927	117.62	36,270.327
	3rd order	260–570	Y = −2388.8X − 8.4157	0.9201	19.86	15.8640
		570–700	Y = −6797.1X − 2.9193	0.9891	26.51	11,005.481
		700–790	Y = −25,490X + 21.064	0.937	259.21	5.21×10^{16}

3.3. Chemical Characterization of Pyrolysis Chars

3.3.1. Elemental Composition and Atom Conservation

The ultimate analysis of the raw materials and resulting chars outlined a trend of carbon enrichment alongside heteroatom depletion as a function of thermal severity (Tables 3 and 4). For lignite (C-series), carbon content jumped from 47.02 wt% in the raw material to 77.29 wt% at 650 °C (120 min), while hydrogen dropped monotonically from 3.48 wt% to 1.20 wt%.

At any given set of processing parameters, the ultimate carbon and hydrogen concentrations in leonardite chars (L-series) were lower than those of their lignite counterparts. Most notably, the sulfur content within leonardite chars remained highly resilient or increased with temperature (peaking at 2.09 wt% at 650 °C), which is roughly double the sulfur retention found in corresponding lignite chars. This indicates that the sulfur and remaining oxygen atoms within the weathered leonardite matrix are deeply integrated into stable, complex aromatic heterocyclic networks, making them highly resistant to thermal evolution under standard inert pyrolysis regimes.

Table 3. Ultimate analysis of lignite char.

Sample	N [%]	C [%]	H [%]	S [%]	O [%]	O/C Ratio	C/N Ratio	H/C Ratio
C-Raw	0.17 ± 0.01	47.02 ± 0.19	3.48 ± 0.32	1.04 ± 0.25	15.75 ± 0.25	0.33 ± 0.01	274.84 ± 14.89	0.07 ± 0.01
C-450-30	0.30 ± 0.14	70.44 ± 1.17	2.81 ± 0.08	0.49 ± 0.10	9.76 ± 1.49	0.14 ± 0.02	302.40 ± 138.00	0.04 ± 0.00
C-450-120	0.50 ± 0.03	62.63 ± 0.74	2.50 ± 0.23	0.51 ± 0.07	12.80 ± 0.87	0.20 ± 0.02	126.95 ± 7.80	0.04 ± 0.00
C-650-30	0.43 ± 0.01	71.41 ± 0.65	1.44 ± 0.13	0.41 ± 0.05	8.55 ± 0.72	0.11 ± 0.01	164.11 ± 8.06	0.02 ± 0.00
C-650-120	0.36 ± 0.11	77.29 ± 2.62	1.20 ± 0.12	0.65 ± 0.10	1.22 ± 0.34	0.02 ± 0.01	238.70 ± 80.15	0.02 ± 0.00
C-850-30	0.35 ± 0.03	71.93 ± 0.96	0.39 ± 0.07	0.45 ± 0.03	5.13 ± 0.88	0.07 ± 0.01	203.89 ± 6.57	0.01 ± 0.00

Table 4. Ultimate analysis of leonardite char.

Sample	N [%]	C [%]	H [%]	S [%]	O [%]	O/C Ratio	C/N Ratio	H/C Ratio
L-Raw	0.23 ± 0.02	46.87 ± 1.15	3.33 ± 0.31	1.19 ± 0.08	48.39 ± 1.13	1.03 ± 0.03	210.58 ± 6.74	0.07 ± 0.01
L-450-30	0.37 ± 0.01	46.86 ± 1.06	2.16 ± 0.02	1.14 ± 0.375	49.48 ± 1.45	1.06 ± 0.02	128.04 ± 1.24	0.05 ± 0.00
L-450-120	0.35 ± 0.02	56.16 ± 0.37	2.19 ± 0.20	1.00 ± 0.11	40.30 ± 0.66	0.72 ± 0.02	161.45 ± 9.16	0.04 ± 0.00
L-650-30	0.11 ± 0.00	40.30 ± 0.72	0.86 ± 0.15	1.79 ± 0.07	57.00 ± 1.72	1.42 ± 0.04	376.04 ± 0.00	0.02 ± 0.00
L-650-120	0.20 ± 0.1	46.92 ± 2.07	0.75 ± 0.15	2.09 ± 0.44	50.04 ± 1.25	1.07 ± 0.02	309.32 ± 144.78	0.02 ± 0.00
L-850-30	0.21 ± 0.03	64.64 ± 1.17	0.38 ± 0.02	1.51 ± 0.34	33.26 ± 1.22	0.51 ± 0.01	317.65 ± 48.78	0.01 ± 0.00

3.3.2. Van Krevelen Plot for Lignite and Leonardite Chars

The structural transition vectors (H/C and O/C) plotted on the van Krevelen diagram (Figure 6) illustrated the devolatilization profiles of both feedstocks. Lignite chars migrated downwards (for H/C) and leftwards (for O/C) with increasing temperature, a standard trend reflecting systematic demethylation (dropping H/C ratio) and decarboxylation (dropping O/C ratio) [25]. However, leonardite chars showed a profound deviation: their O/C ratios remain remarkably high (1.06 to 1.42) even as temperatures crossed from 450 °C to 650 °C, contrasting sharply with the rapidly deoxygenating lignite vectors. Given that the raw feedstocks possessed comparable initial values, this persistent oxygen retention in the leonardite chars highlights that geological weathering fundamentally changes the underlying organic chemistry. Rather than existing as simple carboxylic groups that easily cleave as CO_2, a large portion of the oxygen in leonardite may be locked into highly stable ether, phenolic, or cross-linked macro-aromatic frameworks that survive mid-to-high temperature carbonization. This makes the resulting leonardite char more reactive due to the high presence of oxygen, a polar element. Consequently, leonardite char is more susceptible to degradation when used in reactivity environments.

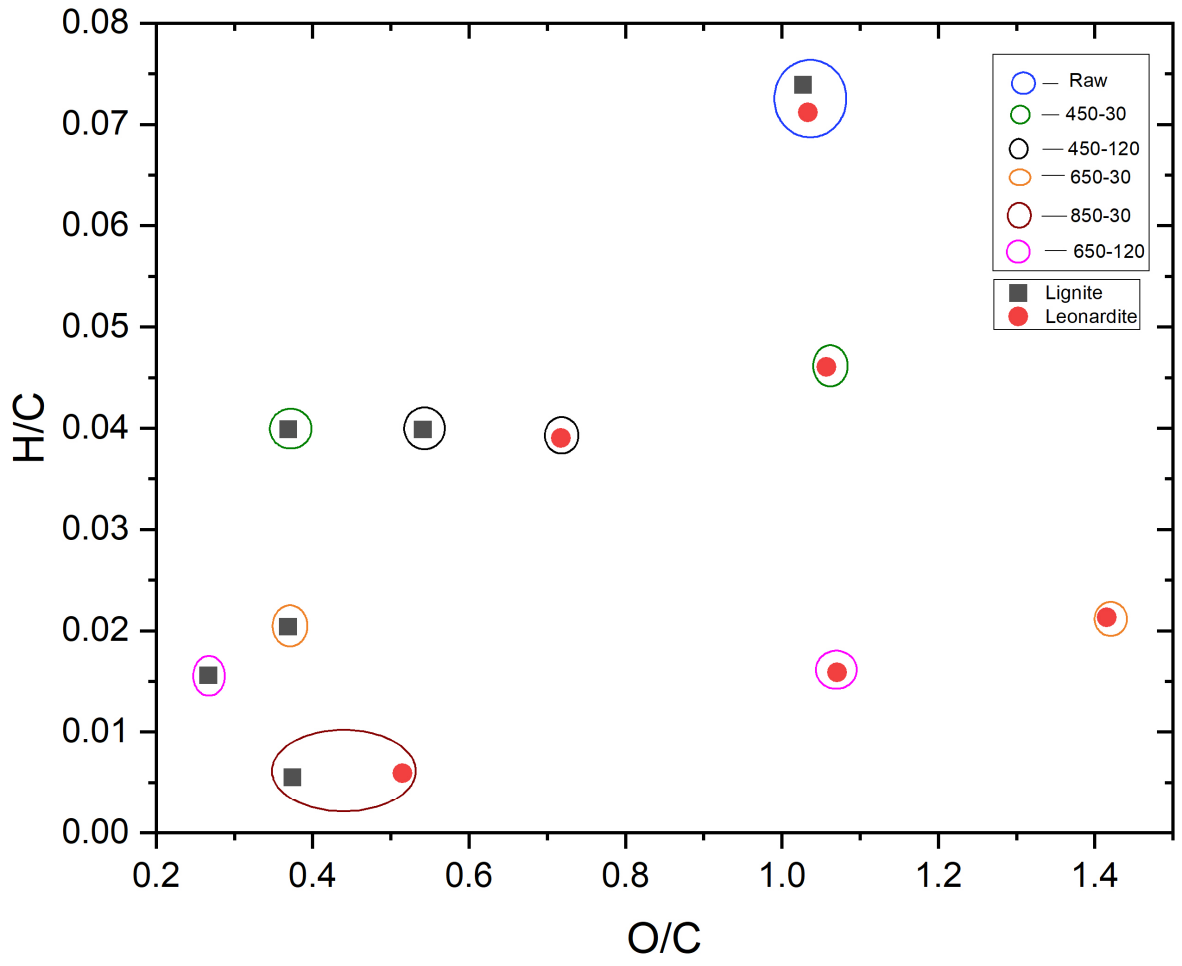


Figure 6. O/C vs. H/C plot (van Krevelen) for leonardite and lignite chars.

4. Conclusions

This study provided a systematic, comparative evaluation of the carbonization kinetics and product distribution of lignite and naturally oxidized leonardite across a wide range of pyrolytic temperatures and

isothermal residence times. By isolating the operational and thermodynamic factors that govern low-rank solid-state transformations, several critical insights were established:

(1) Pyrolysis temperature was confirmed as the dominant factor controlling final product splits, as it dictates the thermodynamic viability of specific chemical bond-cleavage regimes. Isothermal residence time primarily determines the kinetic completeness of these reactions, with its most pronounced effects occurring in lower-temperature windows (450 °C), where primary devolatilization approaches equilibrium at higher thermal thresholds.

(2) While both carbonaceous precursors yielded remarkably identical quantities of solid char residue across all tested variations, their volatile phase architectures split along fundamentally different pathways. Lignite matrices favored the formation of condensable heavy liquids (tar), which peaked distinctly at 650 °C before undergoing severe secondary gas-phase cracking at 850 °C. Conversely, leonardite consistently minimized liquid yields while maximizing light, permanent gas evolution, highlighting an inherently weathered structure dominated by lighter organic fractions.

(3) Macro-kinetic modeling via the Coats-Redfern method demonstrated high effectiveness for primary devolatilization stages under first-order assumptions, confirming that leonardite consistently requires lower apparent activation energies (5–26 kJ/mol) than lignite (12–32 kJ/mol) up to 700 °C. However, the analysis also exposed the limitations of the Coat-Redfern method at elevated temperatures (700–800 °C), where third-order assumptions and secondary polycondensation windows yielded steeply elevated activation energies (up to ~296 kJ/mol for lignite and ~259 kJ/mol for leonardite) likely driven by intra-particle mass-transfer limitations and gas-phase diffusion rather than single-step bond scission.

(4) Solid char characterization demonstrated that while lignite-derived chars achieve higher absolute carbon enrichment, leonardite-derived chars maintain double the relative sulfur concentration. Furthermore, van Krevelen atomic migration vectors proved that a substantial portion of leonardite's structural oxygen remains locked within highly stable cross-linked aromatic, phenolic, or ethereal configurations that strongly resist thermal de-functionalization even up to 650 °C.

These findings establish a clear predictive framework for the thermochemical optimization of local low-rank coal deposits. While lignite presents an excellent precursor for synthetic liquid fuels and highly structured carbonaceous adsorbents, the lower activation energy barriers, high gas reactivity, and oxygen-resilient char matrix of leonardite unlock its unique potential for target-driven applications in advanced syngas production, specialized catalytic platforms, and functional environmental remediation media.

Author Contributions

J.T.O.: data curation, writing—original draft preparation, methodology, investigation, validation, software, visualization; H.I.: conceptualization, writing—reviewing and editing, supervision, methodology, validation, funding acquisition, resources. All authors have read and agreed to the published version of the manuscript.

Funding

This research was funded by Videre Energy Ltd., through the Mitacs Accelerate contract (IT39486).

Institutional Review Board Statement

Not applicable.

Informed Consent Statement

Not applicable.

Data Availability Statement

Data available upon request.

Acknowledgments

We acknowledge our industrial partner, Videre Energy Ltd., for providing funding for this project through the Mitacs Accelerate contract (IT39486). We are grateful to the Clean Energy Technologies Research Institute (CETRI) at the University of Regina for providing the research infrastructure essential for this study.

Conflicts of Interest

The authors declare no conflict of interest.

Use of AI and AI-Assisted Technologies

During the preparation of this work, the authors used Grammarly and Microsoft Copilot to improve the readability of the Manuscript. After using these tools, the authors reviewed and edited the content as needed and take full responsibility for the content of the published article.

References

1. Ofoe, J.T.; Yusuf, M.; Ibrahim, H. A review on coal pyrolysis and gasification: Understanding the chemistries and influence of operating conditions. *Clean Energy* **2025**, *9*, 3–21. https://doi.org/10.1093/ce/zkaf021.
2. Xie, K.C. Coal Pyrolysis Reactions. In *Structure and Reactivity of Coal*; Springer: Berlin/Heidelberg, Germany, 2015; pp. 119–179. https://doi.org/10.1007/978-3-662-47337-5_4.
3. Girhe, P.; Barai, D.; Bhanvase, B. Adsorption of Metals Using Activated Carbon Derived from Coal. In *Clean Coal Technologies*; Springer International Publishing: Cham, Switzerland, 2021; pp. 233–265. https://doi.org/10.1007/978-3-030-68502-7_10.
4. Sabzehmeidani, M.M.; Mahnaee, S.; Ghaedi, M.; et al. Carbon based materials: A review of adsorbents for inorganic and organic compounds. *Mater. Adv.* **2021**, *2*, 598–627. https://doi.org/10.1039/d0ma00087f.
5. Schobert, H. Synthesis. In *Rethinking Coal: Chemicals and Carbon-Based Materials in the 21st Century*; Oxford University Press: Oxford, UK, 2022; pp. 174–189. https://doi.org/10.1093/oso/9780199767083.003.0012.
6. Wu, D.; Zhang, W.; Fu, B.; et al. Chemical structure and gas products of different rank coals during pyrolysis. *J. Therm. Anal. Calorim.* **2019**, *136*, 2017–2031. https://doi.org/10.1007/s10973-018-7877-4.
7. Ozdoba, D.M.; Blyth, J.C.; Engler, R.F.; et al. Leonardite and humified organic matter. In *Humic Substances: Structures, Models and Functions*; Royal Society of Chemistry: Cambridge, UK, 2001; pp. 309–314. https://doi.org/10.1039/9781847551085-00309.
8. Broughton, P.L. Identification of leonardite, a naturally oxidized lignite, by low-angle X-ray scattering method. *J. Sediment. Res.* **1972**, *42*, 356–358. https://doi.org/10.1306/74d7254f-2b21-11d7-8648000102c1865d.
9. Sun, S.; Xu, D.; Wei, Y.; et al. Influence laws of operating parameters on coal pyrolysis characteristics. *J. Anal. Appl. Pyrolysis* **2022**, *167*, 105684. https://doi.org/10.1016/j.jaap.2022.105684.
10. Dai, F.; Zhang, S.; Luo, Y.; et al. Recent Progress on Hydrogen-Rich Syngas Production from Coal Gasification. *Processes* **2023**, *11*, 1765. https://doi.org/10.3390/pr11061765.
11. Makaryan, I.A.; Salgansky, E.A.; Arutyunov, V.S.; et al. Non-Catalytic Partial Oxidation of Hydrocarbon Gases to Syngas and Hydrogen: A Systematic Review. *Energies* **2023**, *16*, 2916. https://doi.org/10.3390/en16062916.
12. Burnham, A.K. Structures of Coal, Kerogen, and Asphaltenes. In *Global Chemical Kinetics of Fossil Fuels*; Springer International Publishing: Cham, Switzerland, 2017; pp. 75–105. https://doi.org/10.1007/978-3-319-49634-4_3.
13. Sarwar, A.; Nasiruddin Khan, M.; Azhar, K.F. Kinetic studies of pyrolysis and combustion of Thar coal by thermogravimetry and chemometric data analysis. *J. Therm. Anal. Calorim.* **2012**, *109*, 97–103. https://doi.org/10.1007/s10973-011-1725-0.
14. Coats, A.W.; Redfern, J.P. Kinetic parameters from thermogravimetric data. II. *J. Polym. Sci. Part B Polym. Lett.* **1965**, *3*, 917–920. https://doi.org/10.1002/pol.1965.110031106.
15. Gao, Z.; Zheng, M.; Zhang, D.; et al. Low temperature pyrolysis properties and kinetics of non-coking coal in Chinese western coals. *J. Energy Inst.* **2016**, *89*, 544–559. https://doi.org/10.1016/j.joei.2015.07.002.
16. Alonso, M.J.G.; Alvarez, D.; Borrego, A.G.; et al. Systematic Effects of Coal Rank and Type on the Kinetics of Coal Pyrolysis. *Energy Fuels* **2001**, *15*, 413–428. https://doi.org/10.1021/ef000170x.
17. Solomon, P.R.; Hamblen, D.G. Pyrolysis. In *Chemistry of Coal Conversion*; Springer: Boston, MA, USA, 1985; pp. 121–251. https://doi.org/10.1007/978-1-4899-3632-5_5.
18. Solomon, P.R.; Serio, M.A.; Suuberg, E.M. Coal pyrolysis: Experiments, kinetic rates and mechanisms. *Prog. Energy Combust. Sci.* **1992**, *18*, 133–220. https://doi.org/10.1016/0360-1285(92)90021-r.
19. Saxena, S.C. Devolatilization and combustion characteristics of coal particles. *Prog. Energy Combust. Sci.* **1990**, *16*, 55–94. https://doi.org/10.1016/0360-1285(90)90025-x.
20. Zhang, S.; Zhu, F.; Bai, C.; et al. Thermal behavior and kinetics of the pyrolysis of the coal used in the COREX process. *J. Anal. Appl. Pyrolysis* **2013**, *104*, 660–666. https://doi.org/10.1016/j.jaap.2013.04.014.
21. Casal, M.D.; Vega, M.F.; Diaz-Faes, E.; et al. The influence of chemical structure on the kinetics of coal pyrolysis. *Int. J. Coal Geol.* **2018**, *195*, 415–422. https://doi.org/10.1016/j.coal.2018.06.014.
22. Wang, T.; Li, C.; Zhou, B.; et al. Experimental investigation of thermal effect in coal pyrolysis process. *Fuel Process. Technol.* **2020**, *200*, 106269. https://doi.org/10.1016/j.fuproc.2019.106269.

23. Xu, Y.; Zhang, Y.; Zhang, G.; et al. Low temperature pyrolysates distribution and kinetics of Zhaotong lignite. *Energy Convers. Manag.* **2016**, *114*, 11–19. https://doi.org/10.1016/j.enconman.2016.02.004.
24. Yan, B.H.; Cao, C.X.; Cheng, Y.; et al. Experimental investigation on coal devolatilization at high temperatures with different heating rates. *Fuel* **2014**, *117*, 1215–1222. https://doi.org/10.1016/j.fuel.2013.08.016.
25. Mukome, F.N.D.; Zhang, X.; Silva, L.C.R.; et al. Use of Chemical and Physical Characteristics To Investigate Trends in Biochar Feedstocks. *J. Agric. Food Chem.* **2013**, *61*, 2196–2204. https://doi.org/10.1021/jf3049142.